Analytic structure of a drag-driven confined dust vortex flow in plasma

Modhuchandra Laishram,* Devendra Sharma, and Predhiman K. Kaw
Institute for Plasma Research, Bhat, Gandhinagar, 382428 India
(Received 27 February 2015; revised manuscript received 26 May 2015; published 29 June 2015)

Flow structure of a dust medium electrostatically suspended and confined in a plasma presents a unique setup where the spatial scale of a volumetric drive by the plasma flow might exceed that of the boundaries confining the dust. By means of a formal implementation of a two-dimensional hydrodynamic model to a confined dust flow and its analytic curvilinear solutions, it is shown that the eigenmode spectrum of the dust vortex flow can lose correlations with the driving field even at the low dust Reynolds numbers as a result of strong shear and finer scales introduced in the equilibrium dust vorticity spectrum by the boundaries. While the boundary effects can replace the desired turbulent processes unavailable in this regime, the shear observable in most of the dust vortex flows is identified to have a definite exponent of dependence on the dust viscosity over a substantially large range of the latter. These results and scalings allow quantification of the notion of dusty plasma medium as a paradigm for a wide range of natural flow processes having scales inaccessible to ordinary laboratory experiments.

DOI: 10.1103/PhysRevE.91.063110 PACS number(s): 52.27.Lw, 52.30.Ex, 52.35.We, 51.20.+d

I. INTRODUCTION

Dynamics of particulate medium subjected to randomness associated with stochastic processes, or turbulence in the suspending medium, has been fundamental to the characteristics of transport processes in the nature [1]. While the regime where an assembly of Brownian particles is additionally subjected to a combination of confining potential and sheared flow has been explored in more recent studies [2], a more correlated fluidlike phase of particles was considered in a nonplanar setup relevant to many interesting experiments performed in the plasma state of the matter [3]. Interesting observations of fluidlike dynamics of the dust medium, with micron-size particles electrostatistically suspended in a plasma, are made over the recent past in various laboratory dusty plasma experiments. Dust medium shows fluid-like behavior when suspended in a plasma either under the microgravity [4–6] or in normal conditions when a dust cloud is electrostatically levitated in the plasma and is in the state of free flow [7,8]. Some of the experiments also observed formation of the dust vortex [9–12] in both these conditions; this includes a very recent observation, in our laboratory, of the formation of a complete toroidal dust structure in a glow discharge plasma with a poloidal dust flow [12]. The mechanisms underlying the vortex motion in these experiments include a range of possibilities that result in forces on the suspended dust, either from its direct or indirect interaction with the surrounding plasma [11] or by external means, including boundaries [13,14], radiation [15,16], magnetic field [10], or neutral flow [17–20]. Study of vortex structures in such a complex medium presents an attractive option for analyzing the dynamics of a fluid flow in the limit of very low Reynolds numbers that interacts, volumetrically, with another driver fluid, for example, a background plasma flow of essentially large Reynolds numbers [21]. While such a turbulent drive can result in the driven dust flow exhibiting a corresponding composition of multiple scale lengths, the dust flow must acquire additional length scales from the boundaries that exist and restrict the dust motion (and dimensions) in the majority of dusty plasma setups where the levitated dust medium is kept confined using a variety of confining mechanisms [15,20,22–24].

A number of natural low-Reynolds-number processes that involve flow relative to boundaries share the dynamical regime with dust flow in the plasma, including swimming of microorganisms [25], bacterial turbulence [26], flow of viscoelastic fluids [27], as well as many robust life-saving biotechnology applications based on networks of microchannels to achieve enhanced rates of mixing, reactions, and conduction of fluid flows [28,29], essentially in the absence of the macroscopic turbulence [30]. This diverse range of applications, and the fundamental structure of flow dynamics in the fluids having a microscopic structure, motivated several recent studies of dust vortex flow, including considerable first-principles molecular dynamics simulations [31] and an approach using numerical solutions of the hydrodynamic model involving an incompressible Navier-Stokes equation solvable for the dust fluid vorticity [3] with boundaries.

A typical laboratory dusty plasma setup has an assembly of negatively charged dust particles electrostatically levitated against the gravity by the electronegative sheath formed on the electrode at the bottom, allowing a supersonic plasma to continuously filter through it in order to let the latter reach the electrode. This arrangement, given the slow time scales of response of the dust in the plasma and very low Reynolds number of its flow, resembles a microscopic semipermeable mixing chamber that allows a colloidal solute to gradually dissolve into a solvent filtering through it at a comparatively high Reynolds number. Similar parallels also exist between such a dusty plasma setup and, for example, artery congestion by a cohesive lump of cholesterol, producing blockade to a cardiac valve that would permit the blood flow of higher Reynolds number but disallow the passage of relatively viscous cholesterol. The lump must, in turn, be gradually dissolved in the blood flow in order for the blockade to be cleared.

Under a systematic hydrodynamic formulation of the dust medium suspended in the plasma, studying the analytic structure of the dust vortex flow equilibria that are driven, volumetrically, by a high-Reynolds-number plasma flow (Re $\sim 10^6$ and above [21]) would allow us to address many

*modhu@ipr.res.in

relevant dynamical issues [3], including interactions of dust flow with limiting boundaries at low Reynolds number. The fact that such a boundary phenomenon is essential to many microscopic natural dynamical processes but difficult to analyze in ordinary laboratory experiments, given the microscopic scales involved, makes the dusty fluid suspended in a plasma an excellent macroscopic specimen of these microscopic systems in addition to being a complex medium often displaying spectacular flow dynamics in various laboratory experiments. Harnessing the considerable analytic potential of the emerging field of dusty plasmas requires a more formal and deterministic analytic treatment that can quantitatively characterize the parameter regimes of laboratory dusty plasma experiments that are indeed relevant to useful microscopic situations in nature. Such a systematic hydrodynamic formulation of the macroscopic fluidlike dust dynamics routinely observed in laboratory plasma experiments long has been awaited and was attempted by Laishram *et al.* [3] with the rather simple motivation of obtaining the first two-dimensional (2D) solutions to describe the dust vortex flow observed in the experiments carried out in normal laboratory conditions (e.g., Ref. [12]) as well as in the international space station under microgravity conditions [11]. These first systematic numerical solutions of the formulation, apart from describing the basic dynamical observations, demonstrated that various fundamental analytic aspects of the dust flow dynamics observable in these experiments are strongly related to natural microscopic flow processes and can indeed be exploited or examined more deterministically by means of the adopted formulation if the analytic version of such solutions presenting the vortex flow can be obtained. For example, the scale of the shear observable in the dust vortex motion relates to the (often overlooked) physics of the boundary phenomena and must follow a definite scaling with respect to the fundamental parameters of the dynamics, e.g., the kinematic viscosity μ of the medium displaying them. It thus becomes clear that once such an analytic characterization is accomplished, more meaningful experiments can be performed where the macroscopic dynamics of the dusty fluid in the laboratory experiments can directly correlate to the microscopic flow processes in the nature that are often out of bounds of the ordinary laboratory experiments.

Unlike the usual driven flow setups, the boundaries confining dust in plasma are exclusively seen by the dust medium while the medium providing the direct volumetric drive is allowed to have a global flow profile. This unique physics aspect of the dusty plasma systems, apart from making it relevant to numerous microscopic semipermeable flow setups in nature, enters the basic mathematical structure of the formulation. Its solution, in turn, is complicated by the inhomogeneity introduced by the driver modes that are not essentially the eigenmodes of the confined dust flow. Showing that the analytic solutions of the equilibrium are yet obtainable in the region of confinement with the driving plasma flows having spatial nonuniformities, the results for the cases with the prescribed vorticity spectrum of the driving plasma flow are obtained in the present treatment. The solutions are characterized to show that the shear scales in the dust vortex flow observable in the experiments follow a definite scaling with respect to the kinematic viscosity of the dust medium over a substantially wide range of the latter. This quantifies the considerable capacity of the dusty plasma setups to represent a range of low-Reynolds-number natural flow processes with sufficient flexibility. It is additionally shown that the driven flow of the dust medium in a plasma conveniently lies in the linear regime ($\mathrm{Re} \leqslant 1$) of the formalism over a substantially wide parameter range. This property is usually desired in the microscopic flow systems where the fundamental processes of mixing, reactions, and convection must take place with sufficient efficiency without a turbulent dynamics [30] that necessitates dominance of the nonlinear effects, introducing interaction between the normal modes of the dynamics.

In the present paper, the hydrodynamic formulation for an incompressible dust medium confined by a conservative potential in a nonplanar, cylindrical setup is introduced in Sec. II. In Sec. III the boundary value problem is constructed for a dust flow driven by a background plasma flow field having a prescribed eigenmode spectrum of the flow shear. The analytic solutions of the hydrodynamic model are obtained in Sec. IV by treating the boundary value formulation as an eigenvalue problem and by expressing the eigenmodes in terms of a linearly independent set of Bessel modes where both driving and driven flows follow valid flux conservation. The solutions that admit use of a driving plasma flow field with a multiple scale vorticity spectrum allow coupling of a multiple scale plasma flow field to produce an associated, but essentially nonidentical, vorticity scale spectrum for the driven dust flow field. The deviation of spectral characteristics of dust vorticity from that of the driver is analyzed as determined largely by the boundary effects and a set of physical parameters, including the dust kinematic viscosity, the coefficient of neutral friction, and that of the ion drag, acting on the dust fluid. The results are summarized and conclusions are presented in Sec. V.

II. 2D HYDRODYNAMIC FORMULATION OF THE CONFINED DUST FLUID

The setup of the confined dust fluid considered here is identical to the recent experiments where a toroidal dust structure is observed having a poloidal dust flow in a glow discharge plasma [12]. The dust fluid in this setup is suspended in the plasma and spatially confined or localized, effectively by a combination of electrostatic and gravitational fields [3]. In normal laboratory setups the confinement of a dynamic dust medium by a 2D or 3D conservative field $\mathbf{F_c} = -\nabla V$ is achievable by use of various experimental means [15,20,22–24]. The electrostatic contribution to the effective potential V can be fairly time independent when both the factors entering the electrostatic Poisson equation, namely the spatial dust density distribution and boundary of the dust medium, are time independent. This equilibrium can still have a strong dynamic character and the associated 2D or 3D steady-state flow field of the driven dust medium is allowed to be both nontrivial and interesting in its nature [11]. The boundaries in many cases may be structured and even self-imposed by a distinct nonfluid or stationary phase of the dust medium having an interface with the fluid phase being analyzed. Considering further the cylindrical setup shown schematically in Fig. 1, with azimuthal symmetry where the confining potential $V(r,z)$ jumps to a very high value V_b at the boundaries of the region

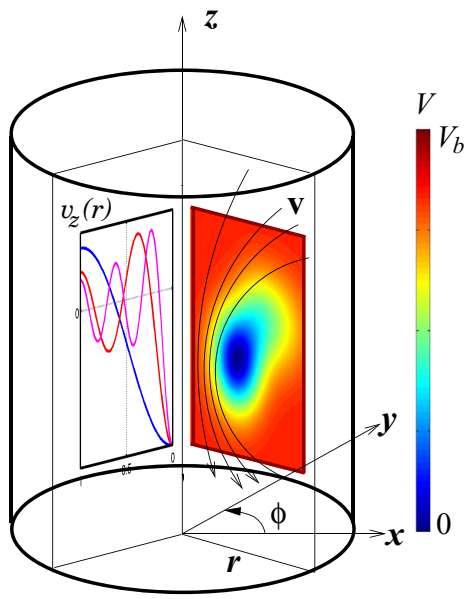

FIG. 1. (Color online) Schematic of the setup in the cylindrical geometry. Surface plot of an example effective confining potential $V(r,z)$ for the dust fluid (surface) is presented along with the flux conserving velocity field vector $\mathbf{v}$ of the unconfined driving fluid in the r-z plane (arrows) and radial profile of its z component $v_z(r)$ (2D plot).

$0 < r/L_r < 1$ and $-1 < z/L_z < 1$ throughout the periodic azimuthal dimension $0 < \phi < 2\pi$, the intersection of the dust volume by an r-z plane is a rectangle.

For a uniform density dust fluid in the above azimuthally symmetric setup, free from any dust source and sink, the basic hydrodynamic equations include the r and z components of the Navier-Stokes equation,

$$\frac{\partial u_r}{\partial t} + u_r\frac{\partial u_r}{\partial r} + u_z\frac{\partial u_r}{\partial z} = -\frac{1}{\rho}\frac{\partial P}{\partial r} - \frac{\partial V}{\partial r} + \mu\nabla^2 u_r - \xi(u_r - v_r) - \nu(u_r - w_r), \quad (1)$$

$$\frac{\partial u_z}{\partial t} + u_r\frac{\partial u_z}{\partial r} + u_z\frac{\partial u_z}{\partial z} = -\frac{1}{\rho}\frac{\partial P}{\partial z} - \frac{\partial V}{\partial z} + \mu\nabla^2 u_z - \xi(u_z - v_z) - \nu(u_z - w_z), \quad (2)$$

and the equation of continuity for the incompressible dust fluid, $\nabla\cdot\mathbf{u} = 0$, written in the cylindrical coordinates as

$$\frac{1}{r}\frac{\partial(ru_r)}{\partial r} + \frac{\partial u_z}{\partial z} = 0. \quad (3)$$

where u is the dust flow velocity, v is the ion flow velocity, and w is the flow velocity of the neutral fluid. P and ρ are the pressure and mass density of the dust fluid, respectively; μ is kinematic viscosity; and ξ and ν are the coefficients of the ion drag and the friction with the neutral fluid acting on the dust [32–34]. For the dust flow which is purely in the r-z plane, the dust vorticity $\omega = \nabla\times\mathbf{u}$ is directed purely along $\hat{\phi}$. In the limit of small Reynolds number $\mathrm{Re} = Lu/\mu$ the nonlinear convective terms in the left-hand sides of Eqs. (1) and (2) are negligible compared to the diffusive terms in the right-hand side and they can be combined to produce the equilibrium equation for ω [3],

$$\mu\nabla^2\omega - (\xi + \nu)\omega + \xi\omega_s = 0, \quad (4)$$

where $\omega_s = \nabla\times\mathbf{v}$ is the vorticity of the ion fluid. In the regime of low Re where the dust flow can be assumed incompressible, defining a stream function ψ such that $\mathbf{u} = \nabla\times(\psi\hat{\phi})$ yields in the cylindrical coordinates,

$$\omega = -\left(\frac{\partial^2\psi}{\partial r^2} + \frac{1}{r}\frac{\partial\psi}{\partial r} - \frac{\psi}{r^2} + \frac{\partial^2\psi}{\partial z^2}\right). \quad (5)$$

Since a multiple mode analysis is desired only along r, following the considerations in Ref. [3] the dependence on z in ψ can be treated via a separable function $\psi_z(z)$ that allows ψ to be expressed in the form of the product $\psi = \psi_r(r)\psi_z(z)$. When the coupling between individual Fourier modes of ψ_z along $\hat{z}$ of the two fluids is considered, the Eq. (4) reduces in a form independent of ψ_z [3],

$$\frac{\partial^4\psi_r}{\partial r^4} + \frac{2}{r}\frac{\partial^3\psi_r}{\partial r^3} - \left[\left(\frac{3}{r^2} + K_1\right) - 2k_z^2\right]\frac{\partial^2\psi_r}{\partial r^2} + \left[\left(\frac{3}{r^3} - \frac{K_1}{r}\right) + \frac{2k_z^2}{r}\right]\frac{\partial\psi_r}{\partial r} - \left[\left(\frac{3}{r^4} - \frac{K_1}{r^2}\right) + \left(\frac{2}{r^2} + K_1\right)k_z^2 - k_z^4\right]\psi_r - K_2\omega_{\mathrm{sr}} = 0, \quad (6)$$

where $K_1 = (\xi + \nu)/\mu$, $K_2 = (\xi/\mu)$ and the source vorticity ω_{sr} is determined by the form of the 2D velocity field $v(r,z)$ of the background ion flow. The above choice amounts to including, for simplicity, only the contribution from the Fourier eigenmodes of the setup along z. The contribution from the modes other than the eigenmodes along z, due to its origin in the inhomegeneity of the formulation, is recoverable as a particular integral over the continuum of the Fourier modes for the cases where the circulations with scale larger than L_z are accounted for. It must, however, vanish in the interior when a sufficiently large number of Fourier eigenmodes are included. The Eq. (6) couples circulations in an unbounded ion flow of finite vorticity on scale L_z to that of the dust fluid confined within the boundaries $-L_z < z < L_z$ and $0 < r < L_r$ while allowing the existence of ion flow circulations of scales larger than L_z. The analytic solutions of the Eq. (6) along r need to be found in terms of eigenmodes of the present setup satisfying the boundary conditions at axial boundaries $\pm L_z$ and radial boundary L_r. We obtain and discuss these solutions in Sec. IV.

III. CONSTRUCTION OF ANALYTIC RADIAL BOUNDARY VALUE PROBLEM IN CYLINDRICAL SETUP

In order to construct the radial solutions bounded in the region $0 < r < L_r$ we begin by casting the Eq. (6) as an eigenvalue problem, with an associated set of eigenfunctions φ_m which satisfy the desired boundary conditions and can be assembled in linear combinations to construct the radial parts of

the driven fluid stream function and the driving fluid vorticity,

$$\psi_r = \sum_{m=1}^{\infty} a_m \varphi_m \quad \text{and} \tag{7}$$

$$\omega_{sr} = \sum_{m=1}^{\infty} b_m \varphi_m, \tag{8}$$

respectively, such that the Eq. (6) is transformed into

$$F \sum_{m=1}^{\infty} a_m \varphi_m = K_2 \sum_{m=1}^{\infty} b_m \varphi_m, \tag{9}$$

with the operator F representing,

$$\begin{aligned} F = {} & \frac{\partial^4}{\partial r^4} + \frac{2}{r}\frac{\partial^3}{\partial r^3} - \left[\left(\frac{3}{r^2} + K_1\right) - 2k_z^2\right]\frac{\partial^2}{\partial r^2} \\ & + \left[\left(\frac{3}{r^3} - \frac{K_1}{r}\right) + \frac{2k_z^2}{r}\right]\frac{\partial}{\partial r} \\ & - \left[\left(\frac{3}{r^4} - \frac{K_1}{r^2}\right) + \left(\frac{2}{r^2} + K_1\right)k_z^2 - k_z^4\right]. \end{aligned} \tag{10}$$

Note that since the driver vorticity $\omega_{\rm sr}$ is prescribed, the coefficients b_m are known. Hence, if the eigenvalues of the operator F corresponding to functions φ_m are known, the coefficients a_m can be determined from (9), producing, in turn, the desired solution (7).

A. Radial boundary conditions and choice of Eigenvectors

The solution procedure requires (i) selection of appropriate of eigenvectors φ_m that satisfy the boundary conditions as well as continuity equation for both, the dust and the ion fluid, and (ii) subsequent expansion of the prescribed source vorticity $\omega_{\rm sr}$ in the linear combination of eigenvectors φ_m. Note that, however, the solutions are sought for the stream function ψ, the physical boundary conditions are essentially defined on the z component of the flow velocity fields of the dust and the ion fluid, chosen in accordance with the relation

$$u_z = \frac{1}{r}\frac{\partial(r\psi)}{\partial r} \tag{11}$$

such that the radial gradient of the eigenfunctions can govern the value of the u_z at the boundaries while in the interior $0 < r < L_r$ it is governed by the source, via Eq. (6). From physical considerations, while in the absence of any physical boundary at $r = 0$, the flow velocity value there is again determined by the driver and only its gradient can be set to zero by symmetry argument; the choice, for example, of a no-slip flow at the outer boundary ($r = L_r$) can be made by setting $u_z(r = L_r) = 0$. This latter choice is made in the present analysis in order to allow for and study the formation of a boundary layer at this boundary.

For most suitable imposition, as discussed below, of the above physical boundary conditions in the present setup, we choose to express the stream functions of both the dust and the background ion flow in terms of φ_m that belong to a set of Bessel functions,

$$\psi_r = \sum_{m=1}^{\infty} a_m J_n\left(\alpha_m \frac{r}{R}\right) \tag{12}$$

and

$$\omega_{\rm sr} = \sum_{m=1}^{\infty} b_m J_n\left(\alpha_m \frac{r}{R}\right). \tag{13}$$

The set $J_n(\alpha_m r/R)$ can additionally be a diagonalized set of eigenvectors by ensuring that the α_m are Bessel zeros, such that the functions φ_m satisfy the orthogonality condition,

$$\int_0^R r J_n\left(\alpha_i \frac{r}{R}\right) J_n\left(\alpha_j \frac{r}{R}\right) dr = \delta_{ij}. \tag{14}$$

Further, since the radial boundary must confine dust with u_r, the stream function ψ must be a constant along z at $r = L_r$ while the radial derivative of the stream function can be controlled to impose an appropriate boundary value of the velocity u_z at this boundary using (11). Accordingly, we choose the set of first-order Bessel functions J_1 (i.e., $n = 1$) as eigenfunctions φ_m that satisfy the $J_n(\alpha_m r/R) = 0$ at both the radial boundaries, $r = 0$ and $r = R = L_r$, while its derivative J_1' can be determined under the following formulation to achieve the solutions with desired boundary flow values.

B. Eigenvalues of the operator F

In order to evaluate the eigenvalues λ_m of F we write the associated eigenvalue equation,

$$(F - \lambda_m) J_1(x_m) = 0, \tag{15}$$

where $x_m = \alpha_m r/R$. Substituting F from (10) in Eq. (15) we get

$$\begin{aligned} & x_m^4 J_1''''(x_m) + 2x_m^3 J_1'''(x_m) - \left[3 + K_1 r^2 - 2r^2 k_z^2\right] \\ & x_m^2 J_1''(x_m) + \left[3 - K_1 r^2 + 2r^2 k_z^2\right] x_m J_1'(x_m) \\ & + \left[-3 + K_1 r^2 - r^4(2/r^2 + K_1)k_z^2 + r^4 k_z^4\right] J_1(x_m) \\ & \quad = r^4 \lambda_m J_1(x_m), \end{aligned} \tag{16}$$

where the prime denotes differentiation with respect to r. Equation (16), upon using the appropriate recurrence relations for the Bessel derivatives and eliminating J_0 and J_2, yields the desired eigenvalues of the operator F,

$$\lambda_m = \left(\frac{\alpha_m}{R}\right)^4 + K_1\left(\frac{\alpha_m}{R}\right)^2 - \left[2\left(\frac{\alpha_m}{R}\right)^2 + K_1\right]k_z^2 + k_z^4. \tag{17}$$

Combining Eq. (9), (15), and (17) produces the equation for the unknown coefficients a_m required for the solutions for the dust flow field in terms of the radial dust stream function ψ_r given by Eq. (12),

$$\sum_{m=1}^{\infty} (\lambda_m a_m - K_2 b_m) J_n(x_m) = 0. \tag{18}$$

Representing sufficiently small scales of the radial variation requires a large number $m = M$ of the eigenfunctions $J_n(x_m)$ for the stream function ψ_r. For the choice of orthogonal set of

finite number of eigenvectors satisfying (14) and a common, nonzero boundary condition for J_1, the coefficients a_m can be determined generally as

$$a_m = \frac{K_2 b_m}{\lambda_m}, \tag{19}$$

whereas the particular boundary conditions can be applied by substituting the value of x_m corresponding to the boundary in the Eq. (18). For the general set of eigenfunctions, independent of condition (14), it is, however, clear that substituting a chosen value $r = r_i$ in Eq. (18) produces a single equation containing total M unknown coefficients a_m. A set of minimum M values, r_i, must therefore be selected to construct a complete set of M simultaneous equations for obtaining the coefficients a_m,

$$\begin{aligned}
&\sum_{m=1}^{M}(\lambda_m a_m - K_2 b_m) J_n(\alpha_m r_1/R) = 0,\\
&\sum_{m=1}^{M}(\lambda_m a_m - K_2 b_m) J_n(\alpha_m r_2/R) = 0,\\
&\cdots\cdots\cdots\cdots\cdots\cdots\cdots\cdots\cdots\cdots\cdots\cdots\\
&\cdots\cdots\cdots\cdots\cdots\cdots\cdots\cdots\cdots\cdots\cdots\cdots\\
&\sum_{m=1}^{M}(\lambda_m a_m - K_2 b_m) J_n(\alpha_m r_M/R) = 0.
\end{aligned} \tag{20}$$

The set of Eqs. (20) can be rearranged in a more familiar form,

$$\begin{bmatrix} A_{11} & A_{12} & \dots & A_{1M} \\ A_{21} & A_{22} & \dots & A_{2M} \\ \vdots & \vdots & \ddots & \vdots \\ A_{M1} & A_{M2} & \dots & A_{MM} \end{bmatrix} \begin{bmatrix} a_1 \\ a_2 \\ \vdots \\ a_M \end{bmatrix} = \begin{bmatrix} B_1 \\ B_2 \\ \vdots \\ B_M \end{bmatrix}, \tag{21}$$

where

$$A_{ij} = \lambda_j J_n(\alpha_j r_i/R) \tag{22}$$

$$\text{and} \quad B_i = K_2 \sum_{j=1}^{M} b_j J_n(\alpha_j r_i/R). \tag{23}$$

The value a_m determined by solution of the set (21) corresponds to the weight of the contribution of m^{th} Bessel mode to the eigenmode spectrum of the dust stream function ψ_r.

C. Implementation of the boundary conditions and the spectral limit

Since the fourth-order Eq. (9) is solved in terms of eigenfunctions that already satisfy two of the required boundary conditions at the boundaries $r = 0$ and R of the cylindrical region, the rest of the procedure clearly admits only two additional boundary conditions which need to be specified in terms of the radial derivatives of the stream function ψ_r at the two radial boundary locations. Note that the cylindrical symmetry of the present setup also results in the eigenmodes J_1 which naturally obey the condition that the radial derivatives of all the physical variables, e.g., that of the velocity u_z, must vanish at $r = 0$. With dust flow velocity at $r = 0$ purely determined by the driving source, no conditions are imposed at this boundary on the u_z value and, in turn, the only remaining boundary condition is applied at $r = R$. Imposing the latter as a no-slip boundary condition, such that the dust flow velocity $u_z = 0$ at $r = R$, and requiring that the solutions must show no oscillations at the scales comparable to the grid resolution, Δr ($< d$, where d is the average particle separation) effectively produces the following two additional equations to replace two equations from the set of Eqs. (20), corresponding, respectively, to r_{M-1} and r_M,

$$\begin{aligned}
&\sum_{m=1}^{M} a_m \frac{\alpha_m}{R} J_{n-1}\left(\alpha_m \frac{r_{M-1}}{R}\right)\\
&\quad - \sum_{m=1}^{M} a_m \left(\frac{\alpha_m}{R}\right)^2 (r_M - r_{M-1}) J_n\left(\alpha_m \frac{r_{M-1}}{R}\right) = 0
\end{aligned} \tag{24}$$

$$\text{and} \quad \sum_{m=1}^{M} a_m \frac{\alpha_m}{R} J_{n-1}\left(\alpha_m \frac{r_M}{R}\right) = 0, \tag{25}$$

with the corresponding matrix coefficients,

$$\begin{aligned}
A_{M-1,j} &= \left(\frac{\alpha_j}{R}\right) J_{n-1}\left(\alpha_j \frac{r_{M-1}}{R}\right)\\
&\quad - \left(\frac{\alpha_j}{R}\right)^2 (r_M - r_{M-1}) J_n\left(\alpha_j \frac{r_{M-1}}{R}\right),
\end{aligned} \tag{26}$$

$$B_{M-1} = 0, \tag{27}$$

and

$$A_{M,j} = \left(\frac{\alpha_j}{R}\right) J_{n-1}\left(\alpha_j \frac{r_M}{R}\right), \tag{28}$$

$$B_M = 0. \tag{29}$$

The desired matrix of Bessel coefficients $\mathbf{a}$ for ψ_r thus can be evaluated as

$$\mathbf{a} = \mathbf{A}^{-1}\mathbf{B}. \tag{30}$$

Determination of $\mathbf{a}$ for a flux conserving plasma flow, which in the present analytic formulation can be prescribed in terms of the source stream function ψ_{sr} or the vorticity ω_{sr}, is thus possible by simply ensuring that the source flow velocities are pure eigenfunctions of the geometric setup. The formulation, however, admits general cases, for example, those treated numerically in Ref. [3] where the dust flow fields were determined to correspond to two cases of source stream functions associated with monotonic and nonmonotonic source velocity profiles. The present analytic formulation reproduces these particular cases by allowing us to express the arbitrary source vorticity functions as a detailed linear combination of the eigenmodes $J_1(x_m)$ represented by Eq. (13).

IV. ANALYTIC STREAM-FUNCTION SOLUTIONS AND CHARACTERIZATION OF DUST FLOW FIELD

The analytic solutions in terms of linear combinations of orthonormal Bessel modes representing the dust stream function can now be obtained provided that the prescribed driving plasma flow field is expressed in the terms of the same set of orthonormal functions such that the coefficients b_m, required to determine the matrix A and B, are known. Considering that for a known function $\omega_{\text{sr}}(r)$ the set of

coefficients b_m can be obtained using the orthonomality condition (14) of the Bessel functions as

$$b_m = \frac{2}{R^2[J_{n+1}(\alpha_m)]^2}\int_0^R r\omega_{sr}(r)J_n\left(\alpha_m\frac{r}{R}\right)dr, \qquad (31)$$

the corresponding set of desired coefficients a_m can be determined using (30) for recovering, for example, the solutions presented in Ref. [3] with two kinds of driver velocity profiles. In the present analysis, however, we limit ourselves to the source vorticities ω_{sr} that are pure eigenfunctions of the cylindrical setup. Additionally, using a single eigenmode as a driver stream function still produces a multiple mode structure of the dust vorticity field in the confinement zone as the resulting dust flow must additionally satisfy the no-slip boundary condition at the boundary $r = R$. The signatures of an associated multiple vorticity scale eigenmode spectrum of the dust flow generated in the resulting boundary layer thus can be analyzed effectively by means of the present analytic eigenmode solutions.

In this bounded setup the diffusive effects included in Eqs. (1) and (2) cause a finite magnitude of the dust flow velocity u in the bulk to reduce in the boundary region and approach zero at the boundary $r = R$. This is despite the flow velocity v of the driving plasma which is finite at the boundary. The corresponding solutions (30), in terms of coefficients a_m, allow us to examine the spectral properties of the dust vorticity field.

The present cases with single-eigenmode structure of the driving plasma flow vorticity ω_{sr}, given by Eq. (13), correspond to the choice

$$b_i = \begin{cases} A_I & \text{if } i = I; \\ 0 & \text{if } i \neq I, \end{cases} \qquad (32)$$

of the ion vorticity while the use of a large number ($M = 200$) of eigenmodes is made to express the resulting dust stream function ψ_r. The first set of analytic solutions is presented in Fig. 2 for the case with $I = 1$ such that the boundary $r = R$ of the confinement zone corresponds to the first zero α_1 of the single eigenmode $J_1(\alpha_1 r/R)$ chosen to represent the ion vorticity, as plotted in Fig. 2(a). The quantities in Fig. 2 and beyond are presented using the system size $L_r = R$ and the ion acoustic velocity U_0 as units of lengths and velocities, respectively. Accordingly, ω and ψ have units U_0/L_r and $U_0 L_r$, respectively. The intensity of the driving velocity field component v_z plotted in Fig. 2(b) scales with the amplitude A_1 of the source vorticity in the confinement domain and has a nonzero value at the boundary $r = R$ as the radial derivative of the stream function ψ_{sr} is nonzero at the boundary for individual eigenmodes for the above choice. The boundary condition of zero dust flow velocity, $u_z(R) = 0$, is, however, ensured by the Eqs. (24) and (25), as plotted in the Fig. 2(d). This boundary condition directly corresponds to the radial derivative of dust stream function, plotted in Fig. 2(c), that approaches zero at the boundary $r = R$.

The complete 2D solutions yielding the stream function $\psi(r,z)$, consistent with the parameter regime associated with a typical laboratory glow discharge argon plasma, are explored below. Considering micron size dust in the plasma with parameters, $n = 10^9\ \mathrm{cm}^{-3}$, $T_e = 3$ eV, and $T_i = 1$ eV, largely at the sheath entrance where ions are streaming with a flow velocity U_0 equivalent to the ion acoustic velocity $c_s = \sqrt{T_e/m_i}$, the value of ion drag coefficient can be estimated to be $\xi \sim 0.2 \times 10^{-5}\ U_0/L_r$ [32–34]. The equilibrium between the two flows is accordingly explored for a range of ion drag coefficient, $\xi = 0.1$, 0.4, 0.7, and $1.0 \times 10^{-5}\ U_0/L_r$. For a typical system size, $L_r \sim 10$ cm, the range of parameter μ can similarly be chosen keeping in view the small Reynolds number ($\sim$1) of the dust flow which is consistent with the linear limit of the model. The resulting 2D solutions are presented in Figs. 3(a), 3(c), and 3(e) for the radial mode numbers $I = 1$, 3, and 5 of the driving plasma vorticity ω_s. These values correspond to the cases where the first, third, and

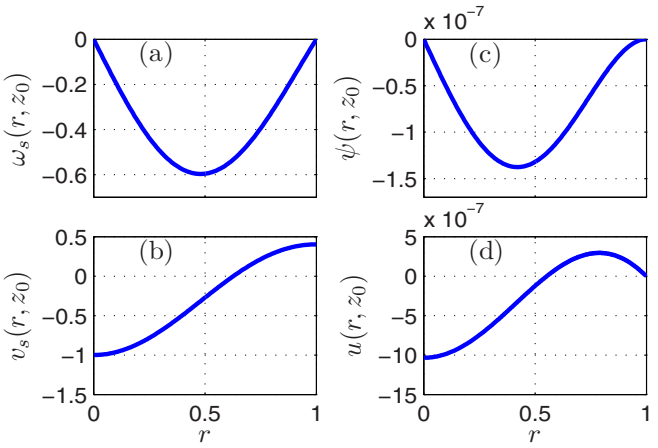

FIG. 2. (Color online) Radial functions for the flow profiles with $I = 1$ at $z = z_0 = 0$. (a) Driver vorticity ω_s, (b) driver velocity v_z, (c) dust stream function ψ, and (d) dust flow velocity u_z for $\mu = 0.1\ U_0 L_r$, $\xi = 10^{-5}\ U_0/L_r$, and $\nu = 0.1\ U_0/L_r$.

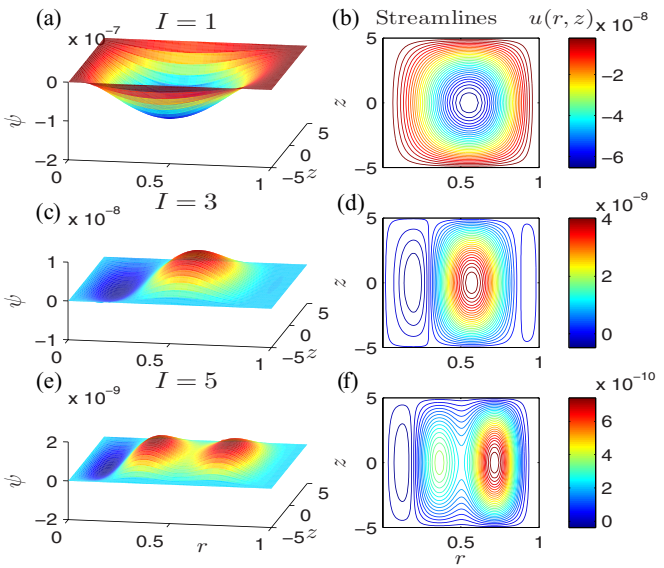

FIG. 3. (Color online) 2D dust stream function $\psi(r,z)$ for single-eigenmode source vorticity with (a) $I = 1$, (c) $I = 3$, and (e) $I = 5$. Dust flow stream lines, or the contours of the product $r\psi$, for single-eigenmode source vorticity with (b) $I = 1$, (d) $I = 3$, and (f) $I = 5$.

fifth zeros of the stream-function eigenmode, J_1, coincide with the boundary location, L_r, respectively. Note that, similarly to the $I = 1$ case presented in Fig. 2, while the radial derivative of the dust stream function also approaches zero, ensuring a zero z component of the dust flow velocity, $u_z = 0$, at the boundary for all these cases, a uniform boundary value of the ψ along $\hat{z}$ also ensures a zero r component for them such that the dust fluid does not cross the radial boundary and is confined in the domain $r < L_r$. The confinement in the region $-L_z < z < L_z$ is similarly ensured by the uniformity of ψ along r at the top and bottom boundaries, $z = \pm L_z$, respectively. The alternate depression and bulges in the surface plots indicate development of vortex structure in the flow velocity field of the dust fluid. These vortices correspond to appearance of circulations in the corresponding stream lines of the dust flow given by the contours of the quantity $r\psi$ that are presented for these cases with $I = 1$, 3, and 5 in Figs. 3(b), 3(d), and 3(f), respectively.

The radial profiles of the driver and the dust velocities at $z = 0$ with increasing value of individual driver mode number I are plotted in Fig. 4 in the left and the middle columns, respectively. The corresponding intensity spectrum of the constituent modes of the driven dust flow vorticity profiles, $\mathrm{Int}(m) = a_m^2$ is plotted in rightmost column of Fig. 4 as a function of the corresponding mode number m. Although a most dominant mode, with the mode number $m = I$ of the driver vorticity ω_s, can be seen in the dust fluid mode number spectrum in each of the cases with $I = 1$, 3, and 5 of the source plotted in Figs. 4(c), 4(f), and 4(i), respectively, a finite intensity at other m values is also recovered in the spectrum of the dust flow. This finite intensity for $m \neq I$ dust modes, unlike source intensity $\mathrm{Int}(m) = \delta_{mI}$, originates from the additional spatial variation of the dust velocity profiles in Figs. 4(b), 4(e), and 4(h) introduced by the no-slip boundary condition, forcing the dust flow velocity to drop to zero at $r = L_r$. Considering

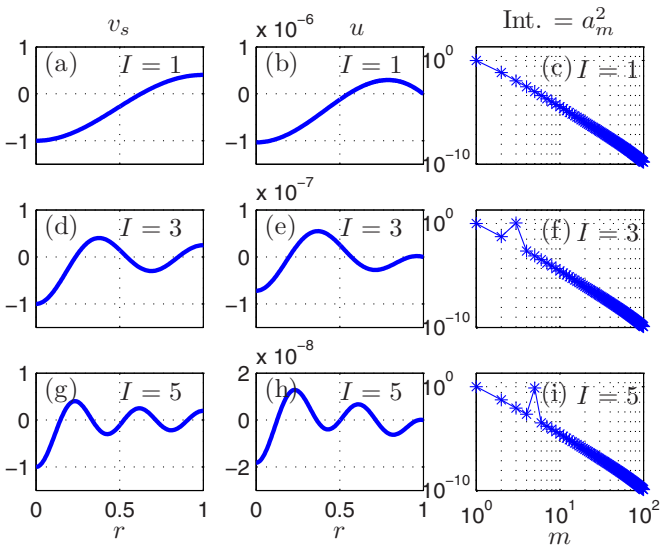

FIG. 4. (Color online) Source flow velocity profile at $z = 0$ for (a) $I = 1$, (d) $I = 3$, and (g) $I = 5$. Dust flow velocity profile at $z = 0$ for (b) $I = 1$, (e) $I = 3$, and (h) $I = 5$. Intensity spectrum for the range of mode number m at $z = 0$ for (c) $I = 1$, (f) $I = 3$, and (i) $I = 5$.

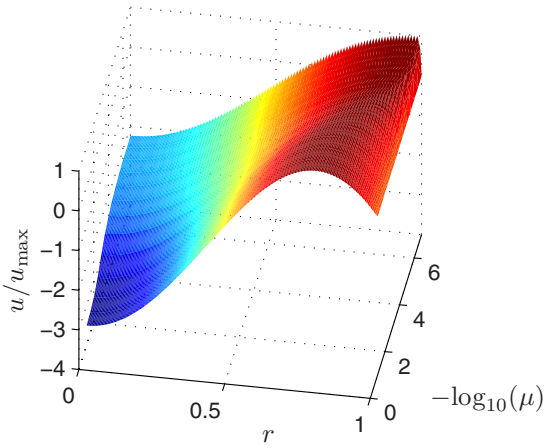

FIG. 5. (Color online) Radial profiles of dust velocity u normalized to the corresponding maximum values $u_{\max}$ appearing at the the edge of the boundary layer whose width shrinks with decreasing μ values, ranging from 10^{-1} to 10^{-7} $U_0 L_r$ arranged on a logarithmic scale.

the above plasma parameters, such that $U_0 \sim 2.5 \times 10^5$ cm s^{-1}, the resulting dust velocities presented in Figs. 4(b), 4(e), and 4(h) agree with the observation of $u \sim 0.1$–1 cm s^{-1} in a typical dust vortex flow experiment [12].

The influence of increasing spatial variation, related to the appearance of a boundary layer, on the dust vorticity spectrum $\mathrm{Int}(m)$ characterizes the correlation between the dust parameters and the intensity of the additional modes with a range of length scales. The width of the boundary layer, effectively the radial interval between the dust flow velocity maximum and the boundary location, reduces gradually with a decreasing value of dust viscosity μ as visible in the radial variation of the dust flow velocity profile plotted in Fig. 5 for $I = 1$ for different μ. The location of the maximum of the normalized velocity is accordingly seen shifting close to the radial boundary $r = L_R$ for the smaller μ, indicating that the boundary layer shrinks and becomes steeper at smaller values of μ, presented in Fig. 5 using a logarithmic scale variation.

The complete intensity spectrum of the constituent modes and the effect of the shrinking width of the boundary layer associated with additional short scale modes that it generates in the intensity spectrum can now be analyzed. The intensity spectrum $\mathrm{Int}(m)$ is plotted in Fig. 6 for the case $I = 1$ and values of coefficient of viscosity $\mu = 10^{-1}, 10^{-3}, 10^{-5}$, and 10^{-7} $U_0 L_r$. As seen from Figs. 5 and 6, steepening of the flow velocity variation at the boundary with decreasing μ corresponds to an increase in the contribution of the radial modes with higher mode number m in the vorticity spectrum. Note, for example, that for the case with $\mu = 0.1$ (plotted with "*" in Fig. 6), where the width of the boundary region approximately corresponds to the scaled interval between the zeros of $m = 2$ mode, there is a considerable intensity of $m = 2$ mode in the spectrum. This intensity of the $m = 2$ mode, however, can be seen to drop with reduction in the μ value, whereas the corresponding intensity of the modes with large m increases. This transition is seen accompanied by a proportional reduction in the width of the boundary

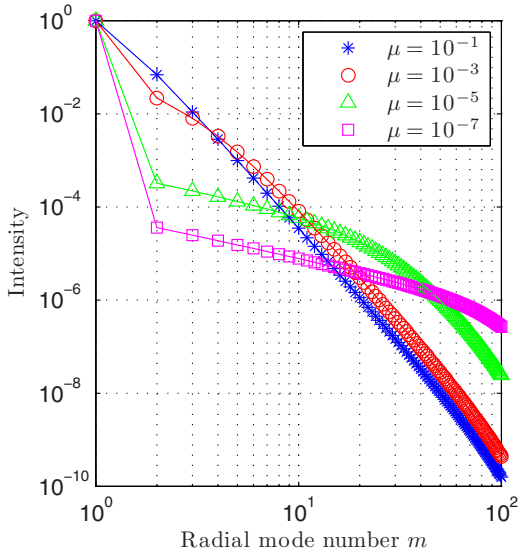

FIG. 6. (Color online) Intensity spectrum for the solutions with $I = 1$, normalized to the intensity a_1^2 of the dust vorticity mode number $m = 1$ for the cases with the value of viscosity coefficient $\mu = 10^{-1}$, 10^{-3}, 10^{-5}, and 10^{-7}.

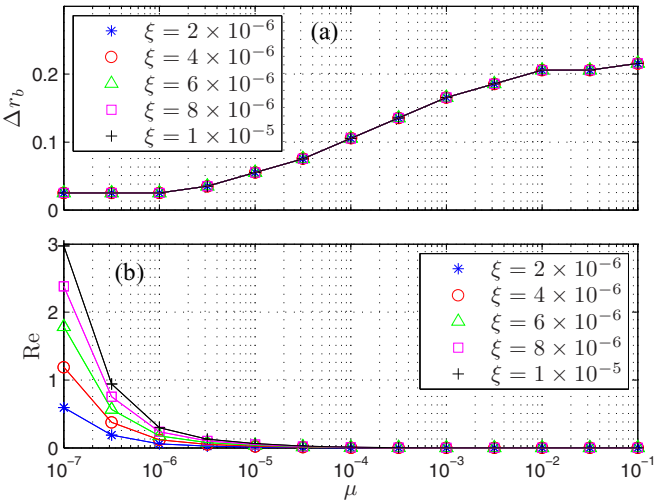

FIG. 7. (Color online) (a) Width Δr_b of the boundary layer and (b) values of the Reynolds number Re for $I = 1$ and the cases with various values of ξ.

layer that rather corresponds to the shorter scale lengths associated with the large m modes ($m > 2$) whose intensity, relative to the $m = 2$ mode, indeed grows for smaller μ values. The mode-number spectrum for varying values of μ, displaying a dominant intensity of resonant scale and a continuum of small scales, features a single exponent for large values of μ but two distinct exponents for small μ values. This indicates that in the regime when the boundary layer is wider and has scale length comparable to that of the driver flow the driver flow introduces a set of structures in the flow having a definite power law with a single exponent. However, in the regime where a thin boundary layer emerges, the boundary may introduce a set of intermediate scales with an exponent which can significantly differ from that of the set of modes generated by the driver flow. Very small length scales that are either comparable or finer than the average inter-dust-particle separation, d, are obviously disallowed in the existing macroscopic model by the conditions (24) and (25). In presence of viscoelastic effects, with the possibility of finite stochasticity at the microscopic level, such finer scales are likely to be populated by modes with a power law that in recent first-principles computer simulations have been predicted to follow a Kolmogorov-like turbulent scaling [31]. However, how these resulting finer-scale structures must interact with the boundary layer that forms at similar scales remains an interesting question for analytically determining the nature of the spectrum at such finer scales. Correctly addressing this region of spectrum under the hydrodynamic formulation would therefore require extending the present Navier-Stokes model to a generalized hydrodynamic model by including the essential viscoelastic effects.

The width of the boundary layer Δr_b is plotted as function of μ for a range of ξ values in Fig. 7(a) and the corresponding dependence of an effective Reynolds number, described further below, is plotted in Fig. 7(b). The boundary layer thickness for this wide range of μ values is also found to be almost independent of the coefficient of ion drag ξ as evident from Fig. 7(a), where profiles of $\Delta r_b(\mu)$ evaluated with various ξ values are seen to be overlapping. The shear scale length is, in turn, not sensitive to the ξ and the driver strength remains largely decoupled with the characteristics of the dust dynamics. This behavior shows the neutrality of the dust dynamics with respect to the driving mechanism and its strength. The shear scale length does, however, show a strong response to the nonuniformity or the presence of spatial stochasticity in the plasma. This is further examined by means of characterizing the boundary layer width in the cases of higher driver mode numbers, $I = 3$ and 5, in addition to the smallest value $I = 1$ as plotted using a logarithmic scale in Fig. 8. It is evident that the regions of separate exponents of μ are present in every case. The boundary layer width is recovered clearly following a definite exponent $\Delta r_b \propto \mu^{1/3}$ in the small to intermediate orders of μ values, e.g., ranging from 10^{-6}–10^{-2} for the case of $I = 1$. The range of μ exhibiting this definite power law is, however, found to be rather limited in the cases of higher driver mode numbers, for example, in the cases $I = 3$ and 5 presented in Figs. 8(b) and 8(c), respectively. The origin of the observed scaling lies in the dust momentum diffusivity largely balancing the momentum source from the driver in the narrow boundary layer, in which the net dissipation via neutrals approaches marginal values. The Eq. (4) at the boundary layer therefore takes the following limiting form:

$$\mu \nabla^2 (\nabla \times \mathbf{u}) \simeq \xi \nabla \times \mathbf{v}. \tag{33}$$

Considering, for $I = 1$, for example, that in the boundary layer region the radial scale length of variation in the driver plasma velocity is comparable to system size, $|\mathbf{v}|/|\nabla \times \mathbf{v}| = v/v' \sim L_r$, while that of the dust velocity variation approaches the effective boundary layer width, $|\mathbf{u}|/|\nabla \times \mathbf{u}| = u/u' \sim \Delta r_b$, in order to achieve the dust flow velocity $u_b \sim u_0$ at the onset of boundary layer using (33) requires

$$\frac{\mu u_0}{\Delta r_b^3} \simeq \frac{\xi v}{L_r}. \tag{34}$$

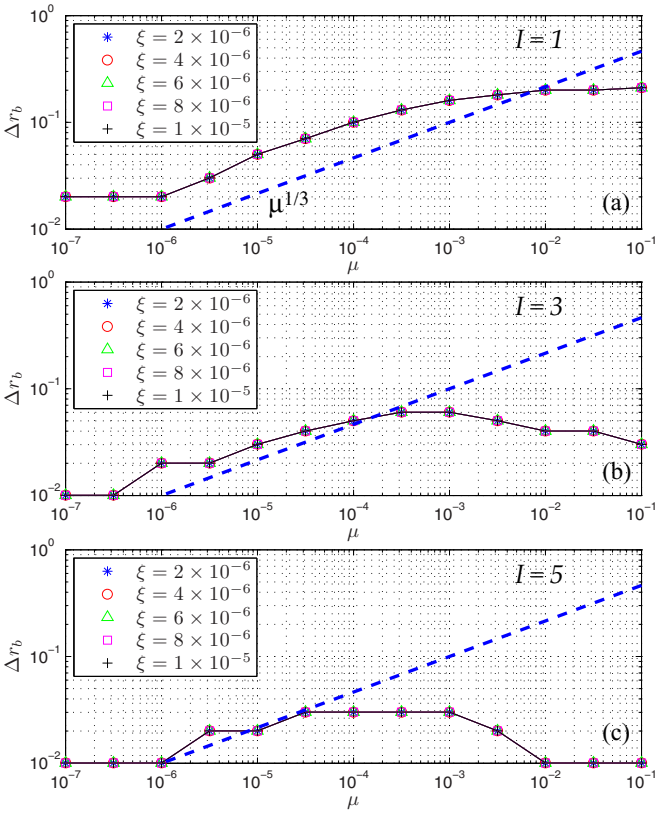

FIG. 8. (Color online) (a) Dependence on μ of width Δr_b of the boundary layer with various values of ξ for the cases with the driver mode number (a) $I = 1$, (b) $I = 3$, and (c) $I = 5$. The broken line represents the dependence $\Delta r_b \propto \mu^{1/3}$.

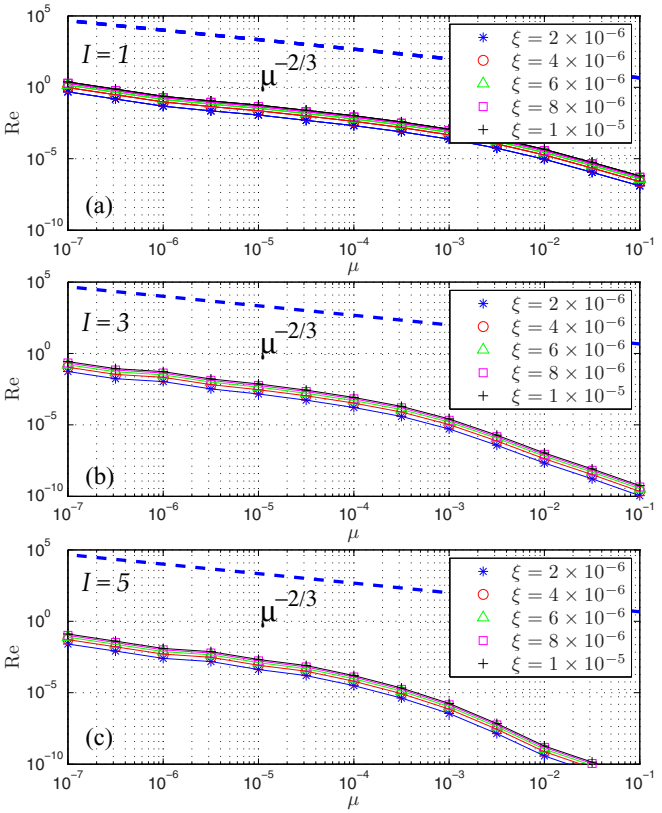

FIG. 9. (Color online) (a) Dependence on μ of the Reynolds number Re with various values of ξ for the cases with the driver mode number (a) $I = 1$, (b) $I = 3$, and (c) $I = 5$. The broken line represents the dependence $\mathrm{Re} \propto \mu^{-2/3}$.

Therefore, treating the quantities ξ, u_0, v, and L_r as parameters would yield the scaling observed in the above characterization,

$$\Delta r_b \simeq \mu^{1/3}. \tag{35}$$

Estimated for $I = 1$, the scaling (35) is, however, obscured by an increasing value of I as seen from Fig. 8, mainly because of the reduction in the values of u_b in comparison to u_0 for $I > 1$ [see Figs. 4(b), 4(e), and 4(h), for example]. The modewise dependence of (35) on μ obtained in the present analysis makes it convenient to determine, from the spectral properties of the driver flow spatial variation present in a particular case, the range in which a corresponding modification of the scaling (35) must be applied. In simpler terms, the considerable range of driven setups where the driver background remains largely free of spatial nonuniformities corresponds to a class of systems analytically more tractable by (35) in comparison to those where the flows may rather be driven by autonomous mechanisms for the vortex dynamics, for example, those involving temperature- or charge-density variations within the structure region with sharper gradients. The regime of (35) suitably covers alternate drivers like a thermophoratic force, translating into a force $\gamma_n \omega_n$ by the neutral vorticity field which frictionally couples to dust particles via coefficient γ_n, and other generic mechanisms [18] that effectively yield a nonconservative force field capable of entering Eq. (4).

Another important quantity that can additionally be estimated and examined as function of μ and ξ is the Reynolds number Re. Considering the recovery of an effective boundary layer width, in the form of the interval Δr_b, allows us to define and estimate the effective Reynolds number, $\mathrm{Re} = u_b \Delta r_b / \mu$, for various cases where $u_b = u(r = L_r - \Delta r_b)$. In view of the large range of the parameter μ ($1 < \mu < 10^{-7} U_0 L_r$) explored in the present analysis covering the limit of considerably small μ values, the ratio $u_b \Delta r_b / \mu$ might shoot up unless a corresponding variation is recovered in the product $u_b \Delta r_b$ appearing in the numerator. Using the values of u_b and Δr_b, both of which are the output of the present analysis, it can now be examined whether the values of Re associated with the results presented above are well within the linear limit $\mathrm{Re} < 1$ of the Eqs. (1) and (2) as required in order to reconfirm the applicability of the analysis to the considered low-Reynolds-number setups. The estimated values of Re are plotted in Fig. 7(b) for the range of parameters μ and ξ relevant to the general laboratory dusty plasma and other low-Reynolds-number setups considered in the present analysis. The domain $\mathrm{Re} < 1$ in Fig. 7(b) thus can be considered to represent the linear limit, suitably covered by the present analysis. While sufficiently large values of drag coefficient ξ are admissible at large μ without losing the self-similarity of the solutions, for smaller values of μ a corresponding limiting ξ value

can be estimated by finding the curve Re(μ) that intersects the horizontal line Re = 1 at the chosen μ. A dependence is recovered in Re < 1 profiles over the viscosity μ with a definite exponent where Re $\propto \mu^{-2/3}$ that suitably follows from the scaling (35), as Re $= u_b \Delta r_b/\mu$, hence Re $\sim \mu^{-2/3}$. This dependence, as presented in the logarithmic plots in Fig. 9, is once again pronounced in a longer range of μ values for the small mode numbers (e.g., $I = 1$) and the profiles show this definite ordering to be obscured by the increasing spatial fluctuation in the driver for larger μ values, for example, in the cases of $I = 3$ and 5. A rather stepwise change in the profiles at small and large μ values in Fig. 8 are caused by the spatial resolution, which is analytically limited by the maximum number M of the dust eigenmodes in use, getting highlighted over the logarithmic scale. It is estimated that for the cases of relatively higher dust charge densities ($\sim 4 \times 10^4\, e^-$) and moderate dust flow velocities ($\sim$0.5 cm s^{-1}) achievable in the existing systems displaying vortex dynamics, the lowest μ value used in the present analysis ($10^{-7}\ U_0 L_r \equiv 0.26\,\mathrm{cm}^2\,\mathrm{s}^{-1}$) approaches the results of the computer simulations yielding the shear viscosity η for the Yukawa systems (e.g., $\mu = \eta/mn \sim 0.5\sqrt{3}\omega_E a^2 \equiv 0.21\,\mathrm{cm}^2\,\mathrm{s}^{-1}$ [35,36], where m and n are dust mass and particle density, respectively; ω_E is the Einstein frequency; and a is the average interdust separation) using the present dusty plasma parameters [12]. For these μ values, the effective Re $= u_b \Delta r_b/\mu \sim 1$ (using $r_b = 0.5$ cm and $u_b = 0.5\,\mathrm{cm\,s}^{-1}$) indicates that the associated cases having Re < 1 can suitably be treated with the present results. A nonlinear extension of the formulation might further extend this applicability regime quite considerably.

V. SUMMARY AND CONCLUSIONS

For the majority of bounded setups of the dust medium suspended in the plasmas with boundaries and friction, we have analytically addressed the issue that in presence of a background high-Reynolds-number driving plasma flow, what are the characteristics of the 2D driven flow structure and how do the spectral properties of the driver flow influence equilibrium mode number spectrum of the driven flow it is when subjected to important boundary phenomena. For the analysis of driven confined dust fluid vortex flow a boundary value problem was constructed in a nonplanar, cylindrical geometry in terms of dust flow stream function.

The presented analytic treatment used the description of the vorticity of both the dust and of the driving plasma in terms of strength of eigenmodes of a curvilinear bounded setup in the mode-number space. The analytic solutions for the dust flow are obtained by treating the boundary value formulation as an eigenvalue problem and using the linearly independent set of Bessel functions as eigenmodes that allow both driving and driven flows to follow valid flux conservation and have a multiple scale vorticity spectrum. This choice allows a multiple scale plasma flow field to produce a vorticity scale spectrum for the driven dust flow field, essentially nonidentical to the driver and the one that accommodates the effects of boundary with the stationary dust. The spectral characteristics of dust vorticity at higher mode numbers is shown to be determined predominantly by the boundary effects that have additional impact when combined with variation in the usual physical parameters of the dust medium, including the kinematic viscosity and the coefficients of neutral friction and ion drag acting on the dust fluid. Among these effects is the formation of a boundary layer whose width depends on the viscosity and allows the dust flow to be in the low-Reynolds-number regime up to considerably smaller values of the coefficient of the dust viscosity.

With the effect of increasing complexity in the driver setup resolved in the orthogonal eigenfunctions and characterized individually with increasing mode number, the independence of effects associated with boundary could be identified and shown to have definite exponents of variation with respect to the medium viscosity μ. While the effective boundary layer width is recovered to scale with $\mu^{1/3}$, the effective Reynolds number for the setup is recovered to scale with $\mu^{-2/3}$. Both of these orderings are seen to be obscured by an increasing spatial complexity of the driving mechanism. The degree of the impact of this complexity is estimated by systematically characterizing the effect of individual driver flow modes in various cases with an increasing value of the cylindrical mode number.

We conclude by discussing that while the regime relevant to present results includes the low-Reynolds-number processes driven by the factors involving spatial complexity and the microscopic setups that are dominated by the boundary effect, following the present implementation of the 2D model, the analysis of additional regimes covered by dusty plasmas must now be more accessible. For example, the regime of stronger coupling where the granularity effects persist in the flowing medium and the Navier-Stokes model can perhaps be modified to cover additionally the dynamics of driven viscoelastic flows [37]. It is also of future interest to investigate the vorticity spectrum structure in the nonlinear limit and explore also its stability such that the possibility of a turbulent spectrum correlating with the boundary effects in the rather relevant nonplanar bounded setups can be addressed more deterministically.

[1] A. Einstein, Ann. Phys. **17**, 549 (1905).
[2] L. Holzer, J. Bammert, R. Rzehak, and W. Zimmermann, Phys. Rev. E **81**, 041124 (2010).
[3] M. Laishram, D. Sharma, and P. K. Kaw, Phys. Plasmas **21**, 073703 (2014).
[4] G. E. Morfill, H. M. Thomas, U. Konopka, H. Rothermel, M. Zuzic, A. Ivlev, and J. Goree, Phys. Rev. Lett. **83**, 1598 (1999).
[5] V. E. Fortov, O. S. Vaulina, O. F. Petrov, V. I. Molotkov, A. V. Chernyshev, A. M. Lipaev, G. Morfill, and H. Thomas, JETP Lett. **96**, 704 (2003).
[6] A. P. Nefedov, G. E. Morfill, V. E. Fortov, H. M. Thomas, H. Rothermel, T. Hagl, A. V. Ivlev, and M. Zuzic, New J. Phys. **5**, 33 (2003).
[7] G. E. Morfill, M. Rubin-Zuzic, H. Rothermel, A. V. Ivlev, B. A. Klumov, H. M. Thomas, U. Konopka, and V. Steinberg, Phys. Rev. Lett. **92**, 175004 (2004).
[8] M. Rubin-Zuzic, H. Thomas, S. Zhdanov, and G. E. Morfill, New J. Phys. **9**, 39 (2007).
[9] O. S. Vaulina, A. A. Samarian, O. F. Petrov, B. James, and F. Melandso, Plasma Phys. Reports **30**, 918 (2004).

[10] Y. Saitou and O. Ishihara, Phys. Rev. Lett. **111**, 185003 (2013).
[11] H. M. Thomas, G. E. Morfill, V. E. Fortov, A. V. Ivlev, V. I. Molotkov, A. M. Lipaev, T. Hagl, H. Rothermel, S. A. Khrapak, R. K. Suetterlin *et al.*, New J. Phys. **10**, 033036 (2008).
[12] M. Kaur, S. Bose, P. Chattopadhyay, D. Sharma, J. Ghosh, and Y. Saxena, Phys. Plasmas **22**, 033703 (2015).
[13] D. A. Law, W. H. Steel, B. M. Annaratone, and J. E. Allen, Phys. Rev. Lett. **80**, 4189 (1998).
[14] G. Uchida, S. Iizuka, T. Kamimura, and N. Sato, Phys. Plasmas **16**, 053707 (2009).
[15] M. Klindworth, A. Melzer, A. Piel, and V. A. Schweigert, Phys. Rev. B **61**, 8404 (2000).
[16] T. Miksch and A. Melzer, Phys. Rev. E **75**, 016404 (2007).
[17] V. I. Vladimirov, L. V. Deputatova, A. P. Nefedov, V. E. Fortov, V. A. Rykov, and A. V. Khudyakov, J. Exp. Theor. Phys. **93**, 313 (2001).
[18] S. Mitic, R. Sutterlin, A. V. Ivlev, H. Hofner, M. H. Thoma, S. Zhdanov, and G. E. Morfill, Phys. Rev. Lett. **101**, 235001 (2008).
[19] M. Schwabe, L.-J. Hou, S. Zhdanov, A. V. Ivlev, H. M. Thomas, and G. E. Morfill, New J. Phys. **13**, 083034 (2011).
[20] M. A. Fink, S. K. Zhdanov, M. Schwabe, M. H. Thoma, H. Hofner, H. M. Thomas, and G. E. Morfill, Europhys. Lett. **102**, 45001 (2013).
[21] B. D. Scott, in *Plasma Physics, Confinement, Transport and Collective Effects*, edited by A. Dinklage, T. Klinger, G. Marx, and L. Schweikhard (Springer, Berlin, 2005), Chap. 8.
[22] S. Mitic, B. A. Klumov, U. Konopka, M. H. Thoma, and G. E. Morfill, Phys. Rev. Lett. **101**, 125002 (2008).
[23] M. A. Fink, S. K. Zhdanov, M. H. Thoma, H. Hofner, and G. E. Morfill, Phys. Rev. E **86**, 065401 (2012).
[24] O. Arp, D. Block, M. Klindworth, and A. Piel, Phys. Plasmas **12**, 0122102 (2005).
[25] E. Lauga and T. R. Powers, Rep. Prog. Phys. **79**, 1 (2008).
[26] C. W. Wolgemuth, Biophys. J. **95**, 1564 (2008).
[27] L. Pan, A. Morozov, C. Wagner, and P. E. Arratia, Phys. Rev. Lett. **110**, 174502 (2013).
[28] P. Yager, T. Edwards, E. Fu, K. Helton, K. Nelson, M. R. Tam, and B. H. Weigl, Nature **442**, 412 (2006).
[29] T. M. Squires and S. R. Quake, Rev. Mod. Phys. **77**, 977 (2005).
[30] A. D. Stroock, S. K. W. Dertinger, A. Ajdari, I. Mezic, H. A. Stone, and G. M. Whitesides, Science **295**, 647 (2002).
[31] M. Schwabe, S. Zhdanov, C. Rath, D. B. Graves, H. M. Thomas, and G. E. Morfill, Phys. Rev. Lett. **112**, 115002 (2014).
[32] M. S. Barnes, J. H. Keller, J. C. Forster, J. A. ONeill, and D. K. Coultas, Phys. Rev. Lett. **68**, 313 (1992).
[33] S. A. Khrapak, A. V. Ivlev, G. E. Morfill, and H. M. Thomas, Phys. Rev. E **66**, 046414 (2002).
[34] A. V. Ivlev, S. A. Khrapak, S. K. Zhdanov, G. E. Morfill, and G. Joyce, Phys. Rev. Lett. **92**, 205007 (2004).
[35] T. Saigo and S. Hamaguchi, Phys. Plasmas **9**, 1210 (2002).
[36] G. Salin and J.-M. Caillol, Phys. Rev. Lett. **88**, 065002 (2002).
[37] P. K. Kaw and A. Sen, Phys. Plasmas **5**, 3552 (1998).